Comments on: "Heat transfer in a square porous cavity in presence of square solid block" International Journal of Numerical Methods for Heat and Fluid Flow, Vol.29(2), pp.640-656

D. Andrew S. Rees

Department of Mechanical Engineering, University of Bath, Bath BA2 7AY, UK.

✉ D.A.S.Rees@bath.ac.uk

Abstract

Purpose – We discuss the need to attend correctly to (i) the accuracy and (ii) the manner in which the value of the streamfunction is determined when two or more impermeable boundaries are present. This is discussed within the context of the paper by Nandalur et al. (2019), which concerns the effect of a centrally-located conducting square block on convection in a square sidewall-heated porous cavity. Detailed solutions are also presented which allow the streamfunction to take the natural value on the surface of the internal block.

Design/methodology/approach – Steady solutions are obtained using finite difference methods. Three different ways in which insulating boundary conditions are implemented are compared. Detailed attention is paid to the iterative convergence of the numerical scheme and to its overall accuracy. Error testing and Richardson's extrapolation have been used to obtain very precise values of the Nusselt number.

Findings – The assumption that the streamfunction takes a zero value on the boundaries of both the cavity and the embedded block is shown to be incorrect. Application of the continuity-of-pressure requirement shows that the block and the outer boundary take different constant values.

Research limitations/implications – The Darcy-Rayleigh number is restricted to values at or below 200; larger values require a finer grid.

Originality/value – This paper serves as a warning that one cannot assume that the streamfunction will always take a zero value on all impermeable surfaces when two or more are present. A systematic approach to accuracy is described and recommended.

Keywords – Porous media, convection, nonlinear flow, square cavity, embedded solid block, accuracy, finite differences.

Paper type – Research paper.

Nomenclature

C	= heat capacity
$\mathscr{C}$	= circulation strength ($\lvert\psi\rvert_{\max}$)
d	= channel width
g	= gravity
h	= step length
i	= index for grid points in the x-direction
i_1, i_2, j_1, j_2	= indices defining the edges of the block
j	= index for grid points in the z-direction
k	= thermal conductivity
K	= permeability
L	= height and width of the cavity
n	= intervals comprising the block
N	= intervals comprising the cavity
Nu	= Nusselt number
p	= pressure
Ra	= Darcy-Rayleigh number
t	= time
T	= dimensional temperature
u	= horizontal velocity
w	= vertical velocity
x	= horizontal coordinate
z	= vertical coordinate

Greek symbols

α	= diffusivity ratio
β	= expansion coefficient
ϵ	= block to cavity aspect ratio, (n/N)
θ	= temperature
κ	= conductivity ratio
μ	= dynamic viscosity
ρ	= density
ψ	= streamfunction

Subscripts, superscripts, and other symbols

c	= cold
exact	= exact solution
f	= fluid
h	= hot
i, j	= denoting grid points
pm	= porous medium
s	= solid
$\hat{}$	= dimensional quantity
$\bar{}$	= Richardson extrapolate

1 Introduction

There exist very many studies which describe nonlinear free convective flow in porous media and while many different configurations have been studied, so have many different extensions to Darcy's law been considered together with the effects of the presence of non-Newtonian fluids and local thermal nonquilibrium between the phases. The present paper lies within a particular subset which is concerned with the effects of the presence of solid obstacles within the heated cavity. Some of these studies have attempted to emulate a porous medium by embedding a large number of blocks within an otherwise fluid-filled cavity. Should the blocks themselves be porous then this is one way to model a bidisperse porous medium.

The present work considers a configuration consisting of a square cavity with a centrally-placed thermally-conducting solid block surrounded by a porous medium. Recent works of a similar nature include include those of Rees and Nield (2016) who considered a Darcy-Bénard configuration where the cavity was heated from below and the block was placed centrally, of Ebaid and Bataresh (2017) who considered the flow induced by a generally-located hot solid block within a square cavity with cold boundaries, and of Nandalur et al. (2019) who considered a sidewall-heated cavity with a central conducting block. We refer the reader to these papers for potential applications of such configurations.

The numerical solution of such problems using finite difference methods falls into the following two main categories: (i) a primitive variables approach, and (ii) a streamfunction approach. When the blocks are surrounded by a fluid then the full no-slip conditions apply and hence all fluid velocities are zero; thus the streamfunction must be constant and have a zero normal derivative. When the blocks are surrounded by a porous medium, then only the normal velocity is zero and thus the streamfunction is then a constant. It is natural and ubiquitous that this constant is set to zero, and such a condition is perfectly correct for natural convection flow within an impermeable cavity. The question then arises about whether this is the

correct value to use on the boundary of any internal blocks, and a discussion of this forms part of the present paper.

The governing equations are presented in §2 and some details of the numerical scheme are provided in §3. Accuracy considerations are discussed in §4 with reference to previously-published papers on cavitiy flows without a central solid block. In §5 our computations, which allow the streamfunction value on the central block to be computed as part of the solution, are compared with those of Nanadlur et al. (2019), and further computations are presented in §6 in order to acquire a full understanding of the nature of the flow and rate of heat transfer as a function of the governing parameters, namely Ra, the Darcy-Rayleigh number, κ, the conductivity ratio between the block and the porous medium and ϵ, the linear size of the block relative to that of the cavity. Conclusions are given in §7.

2 Governing Equations

We consider convection in a square porous cavity which is maintained at a uniformly hot temperature on its left hand sidewall and at a uniformly cold temperature at its right hand sidewall; see Fig. 1. The lower and upper boundaries are insulated. A square block is embedded centrally within the cavity and at its interface with the porous medium the continuity of temperature and rate of heat flux are imposed. The porous medium itself is assumed to be isotropic with a constant permeability. Flow rates are sufficiently slow that viscous dissipation is negligible and Darcy's law applies. Local thermal equilibrium between the phases and the Boussinesq approximation are both assumed to be valid. We follow the notation of Rees and Nield (2016) and therefore the nondimensional equations of motion are given by,

$$\frac{\partial^2\psi}{\partial x^2}+\frac{\partial^2\psi}{\partial z^2}=\mathrm{Ra}\frac{\partial\theta_{\mathrm{pm}}}{\partial x}, \tag{1}$$

$$\frac{\partial\theta_{\mathrm{pm}}}{\partial t}+\frac{\partial\psi}{\partial x}\frac{\partial\theta_{\mathrm{pm}}}{\partial z}-\frac{\partial\psi}{\partial z}\frac{\partial\theta_{\mathrm{pm}}}{\partial x}=\frac{\partial^2\theta_{\mathrm{pm}}}{\partial x^2}+\frac{\partial^2\theta_{\mathrm{pm}}}{\partial z^2}, \tag{2}$$

$$\begin{aligned} x=0,\ x=1: &\qquad \psi=0,\quad \theta=1-x,\\ z=0,\ z=1: &\qquad \psi=0,\quad \frac{\partial\theta_{\mathrm{pm}}}{\partial z}=0. \end{aligned} \tag{3}$$

We note that Nandalur et al. (2019) defines the streamfunction with the opposite sign, but this is of no consequence in what follows. For the solid block, the corresponding heat transport equation and interface conditions are,

$$\frac{\partial\theta_{\mathrm{s}}}{\partial t}=\alpha\Big[\frac{\partial^2\theta_{\mathrm{s}}}{\partial x^2}+\frac{\partial^2\theta_{\mathrm{s}}}{\partial z^2}\Big], \tag{4}$$

$$\theta_{\mathrm{pm}}=\theta_{\mathrm{s}},\qquad \frac{\partial\theta_{\mathrm{pm}}}{\partial n}=\kappa\frac{\partial\theta_{\mathrm{s}}}{\partial n}. \tag{5}$$

The values, κ and α, are the conductivity and diffusivity ratios, and they are given by

$$\alpha=\frac{k_{\mathrm{s}}(\rho C)_{\mathrm{f}}}{k_{\mathrm{pm}}(\rho C)_{\mathrm{s}}},\qquad \kappa=\frac{k_{\mathrm{s}}}{k_{\mathrm{pm}}}. \tag{6}$$

Finally, the Darcy-Rayleigh number is given by

$$\mathrm{Ra}=\frac{\rho_{\mathrm{f}}g\beta(T_h-T_c)KL}{\mu(k_{\mathrm{pm}}/(\rho C)_{\mathrm{f}})}. \tag{7}$$

The solid block is centred at $(x,z)=(\frac{1}{2},\frac{1}{2})$ and has both its width and height equal to ϵ. The sidewall-heated vertical channel is well-known to be stable to all disturbances; see Gill (1969) and Lewis et al. (1995). It is assumed that the extra restriction brought about by confining horizontal surfaces does not alter the stability characteristics, and that the same is true when considering the presence of a solid obstruction. Thus we assume that the resulting flows are stable and unique.

3 Numerical Method

Given that the region of interest is square and that the solid block is both square and centrally located, the finite difference method uses steps of length, h, in both directions, and the number of intervals used is equal to N, which is an even number. Therefore grid points are defined to be at $x_i = ih$ and $z_j = jh$, where both i and j vary between 0 and N and where $hN = 1$. At this general point in space the numerical solution for the temperature, for example, is written as $\theta_{i,j}$.

The above equations and boundary and interface conditions are solved using a straightforward successive over-relaxation solver to find the nonlinear steady-state solution. Central differences are generally employed for all terms. The chief difficulty for such problems is the determination of the value of the streamfunction on the interface between the solid block and the porous medium. This has been described in great detail in Rees and Nield (2016) and shall not be repeated here for the sake of brevity. However, the method determines the overall change in the pressure from the bottom left corner of the block to the top right corner by taking a path around the block in the two different ways; the setting of these pressure changes to be equal to one another then yields the value of ψ for the block itself. Such a scheme has an old pedigree and was used first by Adlam (1986) who considered the effect of placing hot solid blocks within a rectangular enclosure whose boundary is maintained at a cold temperature. This method has been used successfully by many including Ho et al. (1993), who considered the presence of two solid cylinders within a cylindrical enclosure, and Vabishchevich et al. (1996), who studied the presence of a conducting rectangular block inside a rectangular cavity. An almost identical idea was used in a network model by Jamalud-Din et al. (2010), and by Stella and Guj (1989), who developed the technique for vorticity-velocity formulations.

Given that the sole difference between the problem being solved here and that of Rees and Nield (2016) lies with the thermal boundary conditions of the cavity, it is necessary to say something about how the insulating boundary conditions for $\theta_{\rm pm}$ have been implemented at $z = 0$ and $z = 1$.

At $z = 0$ Eq. (**??**) reduces to

$$\frac{\partial^2\theta_{\rm pm}}{\partial x^2} + \frac{\partial^2\theta_{\rm pm}}{\partial z^2} + \frac{\partial\psi}{\partial z}\frac{\partial\theta_{\rm pm}}{\partial x} = 0, \tag{8}$$

given that ψ is zero on the boundary and that steady-state conditions have been assumed. In general we may write the finite difference stencil for the Laplacian of θ in the form,

$$\nabla^2\theta(x_i, z_j) \simeq \frac{1}{h^2}\begin{pmatrix} 0 & 1 & 0 \\ 1 & -4 & 1 \\ 0 & 1 & 0 \end{pmatrix}\theta_{i,j}, \tag{9}$$

for any internal point within the porous medium (noting that we have dropped the 'pm' subscript for notational simplicity). On the lower boundary, $j = 0$, this expression involves $\theta_{i,-1}$, a so-called fictitious point which lies outside of the computational domain. However, a similar central difference discretisation of the $\partial\theta/\partial z = 0$ boundary condition yields $\theta_{i,-1} = \theta_{i,1}$ and hence the discretisation of the Laplacian in Eq. (**??**) becomes,

$$\nabla^2\theta(x_i, z_j) \simeq \frac{1}{h^2}\begin{pmatrix} 0 & 2 & 0 \\ 1 & -4 & 1 \\ 0 & 0 & 0 \end{pmatrix}\theta_{i,0}, \tag{10}$$

which now only involves only those points which are part of the computational domain.

Clearly the $\partial\theta/\partial x$ term in Eq. (**??**) presents no difficulty, but the $\partial\psi/\partial z$ term may be treated in a variety of ways. The first, which shall be termed Case 1, is to use the first order accurate approximation:

$$\frac{\partial\psi}{\partial z}(x_i, 0) \simeq \frac{\psi_{i,1} - \psi_{i,0}}{h}, \tag{11}$$

where $\psi_{i,0} = 0$. The second is to use the one-sided second order approximation:

$$\frac{\partial\psi}{\partial z}(x_i, 0) \simeq \frac{-0.5\psi_{i,2} + 2\psi_{i,1} - 1.5\psi_{i,0}}{h}. \tag{12}$$

The third begins by first considering the central difference form of Eq. (**??**) at $z = 0$:

$$\frac{1}{h^2}\begin{pmatrix} 0 & 1 & 0 \\ 1 & -4 & 1 \\ 0 & 1 & 0 \end{pmatrix} \psi_{i,0} = \mathrm{Ra}\frac{\partial\theta}{\partial x}(x_i, 0), \tag{13}$$

where we have refrained from approximating the right hand side for now. Given that $\psi = 0$ on $z = 0$, we may rearrange Eq. (**??**) into the form,

$$\psi_{i,-1} = -\psi_{i,1} + h^2\mathrm{Ra}\frac{\partial\theta}{\partial x}(x_i, 0). \tag{14}$$

Using this, we may construct the following second order accurate central difference approximation for $\partial\psi/\partial z$

$$\frac{\partial\psi}{\partial z}(x_i, 0) \simeq \frac{\psi_{i,1} - \psi_{i,-1}}{2h} = \frac{\psi_{i,1}}{h} - \tfrac{1}{2}h\mathrm{Ra}\frac{\partial\theta}{\partial x}(x_i, 0). \tag{15}$$

Omission of the second term on the right hand side of Eq. (**??**) yields the expression corresponding to Case 1, which is of first order accuracy.

To summarise, the full finite difference schemes which we used to replace Eq. (**??**) for the three cases are

$$\text{Case 1:} \quad \frac{1}{h^2}\begin{pmatrix} 0 & 2 & 0 \\ 1 & -4 & 1 \\ 0 & 0 & 0 \end{pmatrix} \theta_{i,0}, + \frac{\psi_{i,1}}{h}\Big(\frac{\theta_{i+1,0} - \theta_{i-1,0}}{2h}\Big) = 0,$$

$$\text{Case 2:} \quad \frac{1}{h^2}\begin{pmatrix} 0 & 2 & 0 \\ 1 & -4 & 1 \\ 0 & 0 & 0 \end{pmatrix} \theta_{i,0}, + \Big(\frac{-\frac{1}{2}\psi_{i,2} + 2\psi_{i,1}}{h}\Big)\Big(\frac{\theta_{i+1,0} - \theta_{i-1,0}}{2h}\Big) = 0, \tag{16}$$

$$\text{Case 3:} \quad \frac{1}{h^2}\begin{pmatrix} 0 & 2 & 0 \\ 1 & -4 & 1 \\ 0 & 0 & 0 \end{pmatrix} \theta_{i,0}, + \frac{\psi_{i,1}}{h}\Big(\frac{\theta_{i+1,0} - \theta_{i-1,0}}{2h}\Big) - \tfrac{1}{2}h\mathrm{Ra}\Big(\frac{\theta_{i+1,0} - \theta_{i-1,0}}{2h}\Big)^2 = 0.$$

Similar expressions may be written for the finite difference approximations at $z = 1$. These different schemes will be compared below.

4 Accuracy Considerations

This section considers the accuracy of the method which we have chosen to use. But first it is worth commenting on the use of comparisons between previously published data as a means for concluding that one's own simulations are accurate. Table 1 contains the values of the Nusselt number which, in the present notation, is defined as

$$\mathrm{Nu} = -\int_0^1 \frac{\partial\theta}{\partial x}\Big|_{x=0} dx, \tag{17}$$

where convection in a square sidewall-heated porous cavity has been considered and where there is no central block.

Table 1: Published values of the Nusselt number at Ra = 10 and Ra = 100

Author	Ra = 10	Ra = 100
Walker & Homsy (1978)		3.097
Bejan (1979)		4.2
Gross et al. (1986)		3.141
Beckermann et al. (1986)		3.113
Manole & Lage (1992)		3.118
Moya et al. (1987)	1.065	2.801
Baytaş & Pop (1999)	1.079	3.16
Saeid & Pop (2004)		3.002
Misiriloglu et al. (2005)	1.119	3.05
Jang et al. (2018)		3.102
Nandalur et al. (2019)	1.1158	3.0764

Different authors quote different numbers of significant figures and the values obtained for Nu vary between 1.065 and 1.119 when Ra = 10 and between 2.801 and 4.2 when Ra = 100. There is very little which can conclude from these data except (i) the suggestion that Nu increases with Ra, which one should anticipate on physical grounds, and (ii) that these authors have not been sufficiently careful about assessing the accuracy of their results. This second statement might seem contentious but there will be an exact value for Nu for any given value of Ra, and good numerical practice should give a value which is close to the exact one. Different numerical methods provide different rates of convergence towards the exact solution as the number of degrees of freedom (e.g. the number of elements, the number of grid points, the number of terms in a Galerkin expansion) increases, and there should be some equivalent to a grid-refinement analysis as an internal check for the numerical accuracy of the solution. Yet it is from Tables such as this that many authors claim 'good agreement' as the sole justification for the correctness of their results. It is rare to see a rigorous internal check of the accuracy of published computed data.

The present paper employs a numerical scheme which has second order accuracy in all its different facets (including the use of the Case 1 approximation above which, despite being formally of first order, is applied to a 1D subset of the 2D problem, and therefore overall second order accuracy is maintained). In addition, the solutions have been iterated down to machine accuracy (we have used double precision Fortran90 in our computations) so that no further improvement in the numerical solution of the difference equation can be obtained, and therefore the finite difference equations may be regarded as having been solved exactly. The second order of accuracy should therefore be reflected in the numerical solutions as the grid is refined.

Tables 2 and 3 show how Nu varies with N, for both Ra = 10 and Ra = 100. We shall compare the data shown in Table 1 with our computed values for all three types of discretisation of the insulating condition for θ which were discussed in §3. Our code, which provides for the presence of an internal solid block, was executed with the block being absent. For these values for Nu, the integral in Eq. (**??**) was evaluated using the trapezium rule, which has second order accuracy, and where $\partial\theta/\partial x$ was approximated by the one-sided difference, $(\theta_{1,j} - \theta_{0,j})/h$, which may also be shown to have second order accuracy due to the symmetries inherent in the governing equations. Our detailed values of Nu and the analysis of them are contained in Tables 2 and 3 for Ra = 10 and Ra = 100, respectively.

Table 2a: The effect of different grid resolutions on Nu when Ra = 10

$N \times N$	Case 1	Case 2	Case 3
20×20	1.0773045	1.0793963	1.0801098
40×40	1.0786332	1.0792527	1.0793760
80×80	1.0789683	1.0791393	1.0791591
160×160	1.0790522	1.0790975	1.0791006
320×320	1.0790732	1.0790850	1.0790854
640×640	1.0790785	1.0790815	1.0790816

Table 2b: Richardson extrapolations on the values of Nu given in Table 2a for Ra = 10

$N \times N$	Case 1	Case 2	Case 3
20×20	1.0790761	1.0792048	1.0791314
40×40	1.0790800	1.0791015	1.0790868
80×80	1.0790802	1.0790836	1.0790811
160×160	1.0790802	1.0790808	1.0790803
320×320	1.0790802	1.0790803	1.0790803

Table 2c: Absolute value of the errors in the values of Nu given in Table 2a for Ra = 10

$N \times N$	Case 1	Case 2	Case 3
20×20	0.0017757	0.0003161	0.0010296
40×40	0.0004470	0.0001725	0.0002958
80×80	0.0001119	0.0000591	0.0000789
160×160	0.0000280	0.0000173	0.0000204
320×320	0.0000079	0.0000048	0.0000052
640×640	0.0000017	0.0000013	0.0000014

Table 3a: The effect of different grid resolutions on Nu when Ra = 100

$N \times N$	Case 1	Case 2	Case 3
20×20	3.0119463	3.0730600	3.1513124
40×40	3.0855229	3.1141034	3.1392753
80×80	3.1048364	3.1156424	3.1215810
160×160	3.1097203	3.1132197	3.1143578
320×320	3.1109448	3.1119682	3.1121620
640×640	3.1112511	3.1115320	3.1115628

Table 3b: Richardson extrapolations on the values of Nu given in Table 3a for Ra = 100

$N \times N$	Case 1	Case 2	Case 3
20×20	3.1100484	3.1277845	3.1352629
40×40	3.1112742	3.1261554	3.1156829
80×80	3.1113483	3.1125258	3.1119501
160×160	3.1113530	3.1115510	3.1114301
320×320	3.1113532	3.1113866	3.1113631

Table 3c: Absolute value of the errors in the values of Nu given in Table 3a for Ra = 100

$N \times N$	Case 1	Case 2	Case 3
20×20	0.0994069	0.0382932	0.0399592
40×40	0.0258303	0.0027502	0.0279221
80×80	0.0065168	0.0042892	0.0102278
160×160	0.0016329	0.0018665	0.0030046
320×320	0.0004084	0.0006150	0.0008088
640×640	0.0001021	0.0001788	0.0002096

Table 2 shall be considered first in some detail. Given that Ra = 10, a small value, then we should expect very good accuracy because nonlinear effects are quite weak. Table 2a shows the computed values of Nu for a large number of different gird resolutions and for the three different cases described earlier. The fact these values are close to unity corroborates the fact that convection is weak. We have chosen to use successive interval-halving because this allows the order of accuracy to be displayed and will also enable us to make definitive statements about the absolute accuracy of the solutions. It is clear even from a quick glance at Table 2a that the values of Nu are converging towards a limit as N, the number of intervals increases. From this Table a rough guess at the value of Nu gives 1.08908 to five decimal places.

Although every aspect of our discretisation has second order accuracy, this may be checked using a ratio test. If we denoted by Nu_N the computed value of Nu with N intervals, and by $\mathrm{Nu}_{\mathrm{exact}}$, the precise value, then second order accuracy means that

$$\mathrm{Nu}_N = \mathrm{Nu}_{\mathrm{exact}} + Ah^2 + Bh^4 + \cdots , \tag{18}$$

where the term with the coefficient, B, could be an h^3 term for other systems of equations. Then we may manipulate solutions for three successive grids in the following way:

$$\frac{\mathrm{Nu}_N - \mathrm{Nu}_{2N}}{\mathrm{Nu}_{2N} - \mathrm{Nu}_{4N}} = 4 + O(h^2), \tag{19}$$

where h is assumed to be small. We note that the numerical value on the right hand side of Eq. (**??**) will generally be 2^α for an order-α method. The first three entries in the Case 1 column of Table 2a (i.e. for N = 20, 40 and 80) yields 3.965 as the precise value of the ratio, which is close enough to 4 to confirm second order accuracy. Values of the ratio in (**??**) get closer to 4 as N increases. This type of information cannot be easily obtained when following the strategy of increasing N by fixed amounts such as N = 20, 30, 40, 50 and so on.

Now that we have confirmed second order accuracy, we may now employ the Richardson extrapolation technique to remove the leading order error term. Given the power series expannsion of the the numerical solution shown in Eq. (**??**), we may write down the following for a computation using $2N$ intervals (or steps of length, $\frac{1}{2}h$),

$$\mathrm{Nu}_{2N} = \mathrm{Nu}_{\mathrm{exact}} + \tfrac{1}{4}Ah^2 + \tfrac{1}{16}Bh^4 + \cdots , \tag{20}$$

where we recall that $Nh = 1$. We may now eliminate the h^2 terms between Eqs. (**??**) and (**??**):

$$\overline{\mathrm{Nu}}_N = \frac{4\mathrm{Nu}_{2N} - \mathrm{Nu}_N}{3} = \mathrm{Nu}_{\mathrm{exact}} - \tfrac{3}{4}Bh^4 + \cdots , \tag{21}$$

and therefore this quantity has fourth order accuracy. Table 2b contains the result of this extrapolation process and it becomes very clear that Nu = 1.079080 to six decimal places; there is some doubt as to whether the seventh decimal place is a 2 or a 3. If we now look back at the data in Table 1 we see that Baytaş and Pop are the only authors to provide a value which is correct to the displayed number of

significant figures. Given that Nu = 1 corresponds to the conduction state, it is clear that the nonlinear contribution to Nu is in error by over 50% in the paper by Misiriloglu et al. (2005).

We have used Nu = 1.0790802 as representing the exact solution in order to create Table 2c which shows the absolute errors in the data given in Table 2a. The reduction in the error by a factor of 4 when h is halved (or N doubled) is now very clear.

From Table 2c we see that Case 2 provides the best solution in terms of accuracy, at least as given by the value of Nu, but a quick examination of the extrapolated values shows that Case 1 is best when Richardson extrapolation is employed. The utility of the error-removal mechanism is underscored by considering the absolute error in the Case 1 value for $\overline{\mathrm{Nu}}_{20}$, which is 0.0000041, which is less than 0.0000079, the value for Nu_{320}, a case which takes very considerably longer to calculate.

The corresponding data for when Ra = 100 are provided in Tables 3a, 3b and 3c. Nonlinear effects are now much stronger, which is why Nu is much larger than 1. The method remains of second order. The Case 1 boundary conditions now yield the most accurate values for both Nu and the extrapolated values. From the Case 1 data in these Tables we can state that Nu = 3.111353, or possibly even Nu = 3.1113532. Upon using this value to obtain the absolute errors, we see that the error in the 640×640 data for Case 1 is roughly 100 times larger for Ra = 100 than it is for Ra = 10. We may conclude that one has to check for accuracy carefully as parameters such as the Darcy-Rayleigh number increases. We also conclude from this that the value of Nu given by Beckermann et al. (1986) for Ra = 100 is the most accurate of all those represented in Table 1. It is also clear that errors are now much larger than they were for Ra = 10 and that convergence towards an 'exact' value requires more resolution when Ra increases..

For Case 2 the computed values of Nu increase at first, as N increases, and then decrease towards the limiting value; this is rather unusual behaviour but it is, no doubt, caused by the lack of resolution of small features in the flow field. In fact if someone were using the Case 2 discretisation, and had incremented the number intervals in an arithmetic progression, and had only gone as far as, say, $N = 100$, then it is entirely possible to conclude erroneously that the grid-independent solution is Nu = 3.116, to three decimal places. This mistaken convergence would not happen if the ratio test were employed on this Case 2 data for $N = 40$, 80 and 160 — the ratio is not only close to a power of 2, but is also negative (-0.635) and therefore this signals that a substantial increase in resolution is required.

The analysis above, which uses both the ratio test and Richardson extrapolation, also relies strongly on having sufficiently accurate solutions of the discretised equations. Tests for convergence which rely solely on the difference between successive iterates will become progressively worse as N increases because convergence is slower. It is much better to use residuals which provide an objective measure of the satisfaction of the finite difference equations. But even this will require some exploratory initial computations to determine how the value of the maximum allowable residual relates to the number of reliable significant figures in the solution. After that the ratio test and Richardson's extrapolation may be used safely.

5 Comparison with Published Work

In this section we shall compare some of our computations for the porous cavity containing a solid block with one of those which appears in Nandular et al. (2019). Specifically, we shall compare different computations for the single case, Ra = 100, $\kappa = 5$ and $\epsilon = 0.25$, which is quite representative. This is a case where boundary layers are just beginning to become distinct on the vertical boundaries when the block is absent, and where the block itself has a thermal conductivity which is 5 times that of the porous medium. One of the reasons why the computations in that paper motivated the present work is that the flow and temperature fields do not satisfy the appropriate symmetries of the problem itself.

Figures 2a and 2b show the isotherms and streamlines from Nandalur et al. (2019), where the location of the solid block has been added by the present author for convenience. The temperature field displays

S-shaped isotherms towards the middle of the cavity, while both the lower left and upper right corners, where the isotherms are compressed a little, mark the beginning of the boundary layer flows along the vertical boundaries. In Fig. 2b the outermost streamlines travel in a clockwise direction all the way around the cavity just inside the boundary; this is the expected direction of circulation because of the action of buoyancy along the vertical walls. However, the streamlines which enclose the solid block correspond to a flow with the opposite circulation. This, we believe, is unphysical for there is no mechanism which induces an anticlockwise flow there. Further Figures of this type in Nandular et al. (2019) show a similar qualitative behaviour even when the block is small; it would be thought that the presence of a small block at the centre of the cavity would have almost no influence on the fully clockwise circulation which arises when the block is entirely absent.

A very recent paper by Rees and Nield (2016) in the present journal has considered the Darcy-Bénard analogue of the present configuration. As mentioned earlier, the value of ψ corresponding to the block was computed as part of the solution in that paper, rather than by having $\psi = 0$ imposed upon it. Figure 2c shows both the streamlines and isotherms which were computed using the previously-described slightly modified version of the code of Rees and Nield (2016). In this Figure we see that there remains a very strong clockwise flow in the annular region between the block and the cavity, the only exception being two lobes to the left and to the right of the block; an extremely weak anticlockwise flow takes place there, the extreme weakness being gauged by the fact that $\psi = 4.3843$ on the block as compared with $\psi_{\max} = 4.4842$ which arises in the middle of both of the lobes. Thus the insistence that $\psi = 0$ on the block has the direct effect of causing an unphysical and strong anticlockwise flow around the block. In fact, the setting of $\psi = 0$ on both the boundary and the block means that there is no overall fluid flux between the two surfaces. To see this, the total upward flow between the left hand surface and the block is,

$$Q = \int_0^{(1-\epsilon)/2} w \, dx = \int_0^{(1-\epsilon)/2} \frac{\partial \psi}{\partial x} \, dx = \psi_{\rm block} - \psi_{x=0}, \tag{22}$$

where the integration has taken place on a suitable horizontal line, $z =$ constant.

A second observation is that there is a substantial difference in the behaviour of the isotherms within the block between those shown in Figs 2a and 2c. In Fig. 2a the distance between the isotherms has hardly changed from that which occurs in the porous medium, whereas those in Fig. 2c are very widely spaced with the block, which is to be expected since the relatively large solid conductivity means that the temperature of the block should be almost uniform.

Figure 2d displays what happens when the present code is modified slightly to impose $\psi = 0$ on the block. Like Fig. 2b we see an unphysical anticlockwise circulation about the block, but our third observation is that Fig. 2d also displays a set of symmetries which are absent in Fig. 2b, namely that

$$\psi(x,z) = \psi(1-x,1-z), \qquad \text{and} \qquad \theta(x,z) = 1 - \theta(1-x,1-z). \tag{23}$$

It is a simple matter to show that the governing nonlinear equations, Eqs. (**??**) to (**??**), also satisfy these symmetries and, in the absence of any instabilities (which generally break at least one symmetry) it is to be expected that all solutions will satisfy Eq. (**??**).

A fourth observation is that, while the isotherms in Fig. 2c display discontinuous slopes at all four of the interfaces between the block and the porous medium, the isotherms at the horizontal interfaces in Fig. 2a exhibit no change of slope, despite there being a thermal conductivity ratio of 5 there. Figure 2e is our attempt to model this incorrect behaviour by insisting on a unit conductivity ratio at the upper and lower interfaces, something which may be done independently of the rest of the computation. The result of this artifice is to introduce quite a large number of isotherms within the solid block, but the symmetry remains.

Figure 2f shows the result of modifying the left hand interface condition to look as though there is a unit conductivity ratio. The resulting isotherm and streamline patterns now bear a strong resemblance to those in Figs. 2a and 2b, respectively, and the necessary symmetries have now been lost.

Thus the computations which are represented by Figs. 2a and 2b exhibit two main errors: (i) an unphysical imposition of $\psi = 0$ on the central block, (ii) the incorrect imposition two or possibly three interface conditions which appear to be equivalent to having equal thermal conductivites either side of the interface. The most obvious manifestation of these difficulties result in the absence of the symmetry which must be present. Closer observation reveals the difficulty with the interface conditions.

The rest of this paper is devoted to a brief presentation of some flows for the unit cavity with a centrally-placed square block but where the streamfunction on the block is computed as part of the solution process rather than being imposed.

6 Numerical Results

6.1 Streamlines and isotherms

Figures 3 to 5 display streamlines and isotherms for four different conductivity ratios and for three different block sizes, but the Darcy-Rayleigh number is fixed at 100 to represent a moderately strong flow. In these computations we have selected a 120×120 grid to show the behaviour of the system. One may consult Table 3c to estimate the errors associated with this choice of grid. Figure 3 shows the case when the block size is $\epsilon = 0.25$. Here we see that the solid block is at almost constant temperature when the conductivity ratio is as large as $\kappa = k_{\rm s}/k_{\rm pm} = 100$. The $\theta = 0.5$ isotherm passes through the block, but the neighbouring ones, for which $\theta = 0.45$ and $\theta = 0.55$, remain well within the porous medium. The flow field itself bears a strong resemblance to that shown in Figure 2c, for which $\kappa = 5$, and there are again very weak recirculations to the right and left of the block. When κ reduces to 5 there is very little change apart from the fact that the $\theta = 0.45$ and $\theta = 0.55$ isotherms now cross the corner of the block.

A further reduction to $\kappa = 1$ sees a further migration of the isotherms into the block, and the fact that $\kappa = 1$ means that the slopes of the isotherms are continuous when passing through the interfaces. A further reducton to $\kappa = 10^{-3}$, for which the solid block is close to being adiabatic, causes the isotherms to congregate within the solid block and the isotherms meet the interface normally from the porous medium side. There is a qualitative change in the shape of the streamlines due to the substantial change in the isotherm pattern, and the recirculating regions have moved in an anticlockwise direction away from beside the mid-height of the block.

When the central block corresponds to $\epsilon = 0.5$, the processes described about become stronger in their effect. Thus when $\kappa = 100$ the use of 20 equally-spaced streamlines now displays the weak recirculations to the left and right of the block. Other than that, the streamlines follow what might be termed the "racetrack" and correspond to a clockwise circulation. When κ has reduced to 10, the increased size of the block is such that five of the isotherms pass through it. The weak recirculations have become weaker, and this trend continues as κ reduces in magnitude still further, with the centres of the recirculations descending on the left side and ascending on the right. In the extreme case where $\kappa = 10^{-3}$ two almost perfectly isothermal regions form directly above and below the block. The contraction of the isotherms towards the block is now such that the range of temperature experienced by the block itself is greater than 0.9, which should be compared with a total drop of 1 from left to right of the full cavity.

When ϵ is as large as 0.75 the siutation becomes more extreme. When $\kappa = 100$ the temperature field mostly varies in the horizontal direction in the vertical porous channel, and, conversely, when κ is small the temperature is almost perfectly uniform in the lower half of the right hand channel, the upper half of the left hand channel, and in approximately 80% of the horizontal channels. There we would expect a very large rate of heat transfer across the cavity when κ is large, and a very small one when κ is small.

For the sake of space we shall not present Figures which represent how the flow and temperature fields evolve as Ra increases. However, it is well-known that thermal boundary layers will eventually develop on the left and right hand walls of the cavity. For the present problem these will not become evident until

they become sufficiently narrow that they fit well within the vertical channels. Therefore the presence of a large block will delay the appearance of boundary layers to larger values of Ra than for the case when there is no central block.

6.2 Rates of Heat Transfer

Figure 6 shows how the Nusselt number varies with the Darcy-Rayleigh number for a selected set of values of ϵ and κ. We note that the slopes of curves are precisely zero when $\mathrm{Ra} = 0$ since the physical problem for negative values of Ra is mathmatically identical to that for postive values. While it is to be expected that Nu increases with Ra on physical grounds (increased buoyancy causes an increased flow rate and then thin thermal boundary layers form at larger values of Ra), it is immediately obvious that the rate of heat transfer through the layer is almost independent of the conductivity ratio when the solid block is small. Part of the reason for this is that the centre of the cavity forms the centre of the circulation and, in the absence of a block, will be close to being stagnant. Therefore the physical presence of a small block does little to change the flow field. But given that the block conducts heat, the local changes to the temperature field will cause small changes in the overall Nusselt number.

One interesting aspect of the Nusselt number curves is the change with Ra of the value of κ which maximises the value of Nu. When Ra is small then large values of κ yield the largest value of Nu. This is due to the fact that the domain is almost purely conductive when $\mathrm{Ra} \ll 1$, and a relatively large thermal conductivity of the block will increase the effective conductivity of the block from what it is when $\kappa = 1$. As Ra rises, there is a gradual transition to $\kappa \ll 1$ having the largest value of Nu. We believe that this is due, at least in part, to the extreme deformation of the isotherms at the bottom-left and top-right of the block which is caused by the mismatch in the conductivities, as mentioned earlier. This naturally induces a local flow which assists in increasing the Nusselt number. We also note that the transition between the extreme values of κ forming the optimum case takes place very rapidly when ϵ is small, but is much more gradual when the block is larger.

Given that the central interest in the present paper is the effect of the presence of the central block, Figure 7 shows explicitly how the Nusselt number varies with the size of the block. In this case we have used a 100×100 grid and therefore ϵ takes values which are exact multiples of 0.02. We also note that those solutions when ϵ is close to 1 have less accuracy than those for smaller values because the flow is constarined to take place within only a few grid points. Therefore the last few data points should be taken as being indicative of the trend.

When $\mathrm{Ra} = 10$ the flow is quite weak and the Nusselt number is dominated by conduction between the hot and cold vertical surfaces. When $\epsilon = 0$, i.e. there is no block, Nu is just above 1, which again confirms the lack of strength of the flow. When ϵ increases, the block gradually fills the cavity, and the Nusselt number responds to the increasing dominance of the conductivity of the block either by increasing when $\kappa > 1$ or by decreasing when $\kappa < 1$. When $\kappa = 1$ we see that the $\mathrm{Nu} \to 1$ as $\epsilon \to 1$, which is consistent with no flow when the cavity is completely filled by the block.

At larger values of Ra again we see the strange reversal in behaviour of Nu which was discussed above. For example, when $\epsilon = 0.5$ for both $\mathrm{Ra} = 100$ and $\mathrm{Ra} = 200$ the value of Nu is larger when $\kappa = 10^{-3}$ than when $\kappa = 100$. However, when ϵ increases from this value towards 1, conduction effects begin to dominate, and therefore when ϵ is as large as 0.9 the larger values of Nu correspond to the larger conductivities of the block.

7 Conclusions

This paper has covered many different aspects. First we considered what is good practice for assessing accuracy. Based on using a very detailed set of ancilliary analyses using interval-halving we obtained

extremely accurate solutions for one specific case of convective flow in a sidewall-heated square cavity. From this we were able to assess how close previously published papers are to those correct values. We recommend, therefore, that one should undertake such ancilliary analyses as an internal check for the accuracy of one's solutions; comparison with published data from other sources, especially where little care has been taken over the accuracy of that data, can only confirm, at best, the quality of one's encoding of the numerical method. The clear message from Table 1 is that such comparisons should never be used to confirm accuracy.

The second aspect was an analysis of the results of Nandalur et al. (2018). The idea for the present paper was conceived when it was observed that those computations of flows with a centrally-placed block (i) did not obey the symmetries that are inherent in the mathematical problem, and (ii) had an unphysical clockwise flow around the central block. Clearly the reviewers of that paper did not notice these features either. This unphysical flow direction around the block was caused by the setting of $\psi = 0$ on both the outer boundary of the cavity and on the interface with the block. The presence of a zero normal velocity does imply a constant value of the streamfunction, but it does not mean that the two streamfunction values are the same. The setting of both to the same value means that an overall zero circulation condition has been imposed unwittingly. Whilst such a difficulty will not arise when using a primitive variables formulation, the methodology devised by Adlam (1986) may be implemented quite easily to allow the streamfunction on the central block to converge towards the correct value.

The third aspect was a brief presentation of the overall properties of the system using Adlam's methodology. We find some apparently anomalous results which state that Nu for a poorly conducting block can be larger than for a highly conducting block, wheras the opposite is true when there is no flow. This unintuitive result is traced to the presence of very strongly deformed isotherms near to two corners of the block when $\kappa \ll 1$, and it is this which increases the flow locally and hence increases heat transfer from the sidewalls.

References

Adlam, J.H. (1986), "Computation of two-dimensional time-dependent natural convection in a cavity where there are internal bodies", *Computers and Fluids* Vol.14(2), pp.141–157.

Baytaş, A.C., Pop, I. (1999), "Free convection in oblique enclosures filled with a porous medium", *International Journal of Heat and Mass Transfer* Vol.42(6), pp.1047-1057.

Beckermann, C., Viskanta, R., Ramadhyani, S. (1986), "A numerical study of non-Darcian natural convection in a vertical enclosure filled with a porous medium", *Numerical Heat Transfer, Part A* Vol.10(6), pp.557-570.

Bejan, A. (1979), "On the boundary layer regime in a vertical enclosure filled with a porous medium", *Letters in Heat and Mass Transfer* Vol.6(2), pp.93-102.

Ebaid, M.S.Y., Bataresh, L. (2017), "Impact of eccentricity on heat transfer in an annular square filled with saturated porous media", *Journal of Porous Media* Vol.20(4), pp.325-348.

Gill, A.E. (1969), "A proof that convection in a porous vertical slab is stable", *J. Fluid Mech.* Vol.35, pp.545-547.

Gross, R.J., Bear, M.R. and Hickox, C.E. (1986), "The application of flux-corrected transport (FCT) to high Rayleigh number natural convection in a porous medium" In: *Proceedings of the 8th International Heat Transfer, San Francisco, USA*

Ho, C.J., Chang, W.S., Wang, C.C. (1993), "Natural convection between two horizontal cylinders in an adiabatic enclosure", *A.S.M.E. Journal of Heat Transfer* Vol.115, pp.158–165.

Jamalud-Din, S.-D., Rees, D.A.S., Reddy, B.V.K., Narasimhan, A. (2010), "Prediction of natural convection flow using a network model and numerical simulations inside an enclosure with distributed solid blocks", *Heat and Mass Transfer* Vol.46, pp.333–343.

Jang, B., Jagadeesha, R.D., Prasanna, B.M.R., Sankar, M. (2018), "Natural convection in an inclined parallelogrammic porous enclosure" In: *Flow and Transport in Subsurface Environment (Springer Transactions in Civil and Environmental Engineering series)* pp.279-303.

Lewis, S., Bassom, A.P., Rees, D.A.S. (1995), "The stability of vertical thermal boundary layer flow in a porous medium", *European Journal of Mechanics B: Fluids* Vol.14, pp.395-408.

Manole, D.M., Lage, J.L. (1992) "Numerical benchmark results for natural convection in a porous medium cavity", In: *Heat and Mass Transfer in Porous Media, ASME Conference, HTD 21655.*

Misirlioglu, A., Baytaş, A.C., Pop, I. (2005), "Free convection in a wavy cavity filled with a porous medium", *International Journal of Heat and Mass Transfer* Vol.48(9), pp.1840-1850.

Moya, S.L., Ramos, E., Sen,M. (1987), "Numerical study of natural convection in a tilted rectangular porous material", *International Journal of Heat and Mass Transfer* Vol.30(4), pp.741-756.

Nandalur, A.A., Kamangar, S., Badruddin, I.A. (2019), "Heat transfer in a porous cavity in presence of a square solid block", *International Journal of Numerical Methods for Heat and Fluid Flow* Vol.29(2), pp.640-656.

Rees, D.A.S., Nield, D.A. (2016), "The effect of an embedded solid block on the onset of convection in a porous cavity", *International Journal of Numerical Methods for Heat and Fluid Flow [25th Anniversary special issue]* Vol.26(3/4), pp.950-976.

Saeid, N.H., Pop, I. (2004), "Transient free convection in a square cavity filled with a porous medium", *International Journal of Heat and Mass Transfer* Vol.47, pp.1917-1924.

Stella, F., Gui, G. (1989), "Vorticity-velocity formulation in the computation of flows in multi-connected domains", *International Journal for Numerical Methods in Fluids* Vol.9, pp.1285-1298.

Vabishchevich, P.N., Chudanov, V.V., Churbanov, A.G. (1996), "Numerical simulation of free convection flows in complex domains", *Mathematical Models and Computer Simulations (in Russian)* Vol.8(1), pp.103–118.

Walker, K.L. and Homsy, G.M. (1978), "Convection in a porous cavity", *Journal of Fluid Mechanics* Vol.87, pp.449-474.

Figures

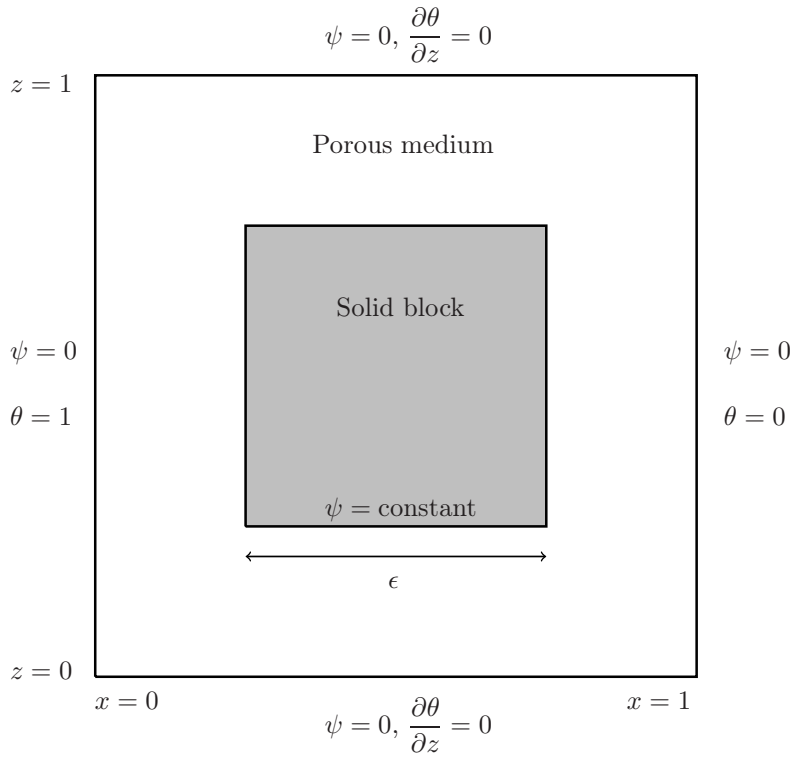

Figure 1: Definition sketch of the porous cavity with a centrally-placed solid conducting block embedded within it. Gravity acts vertically downwards. Nondimensional variables are displayed.

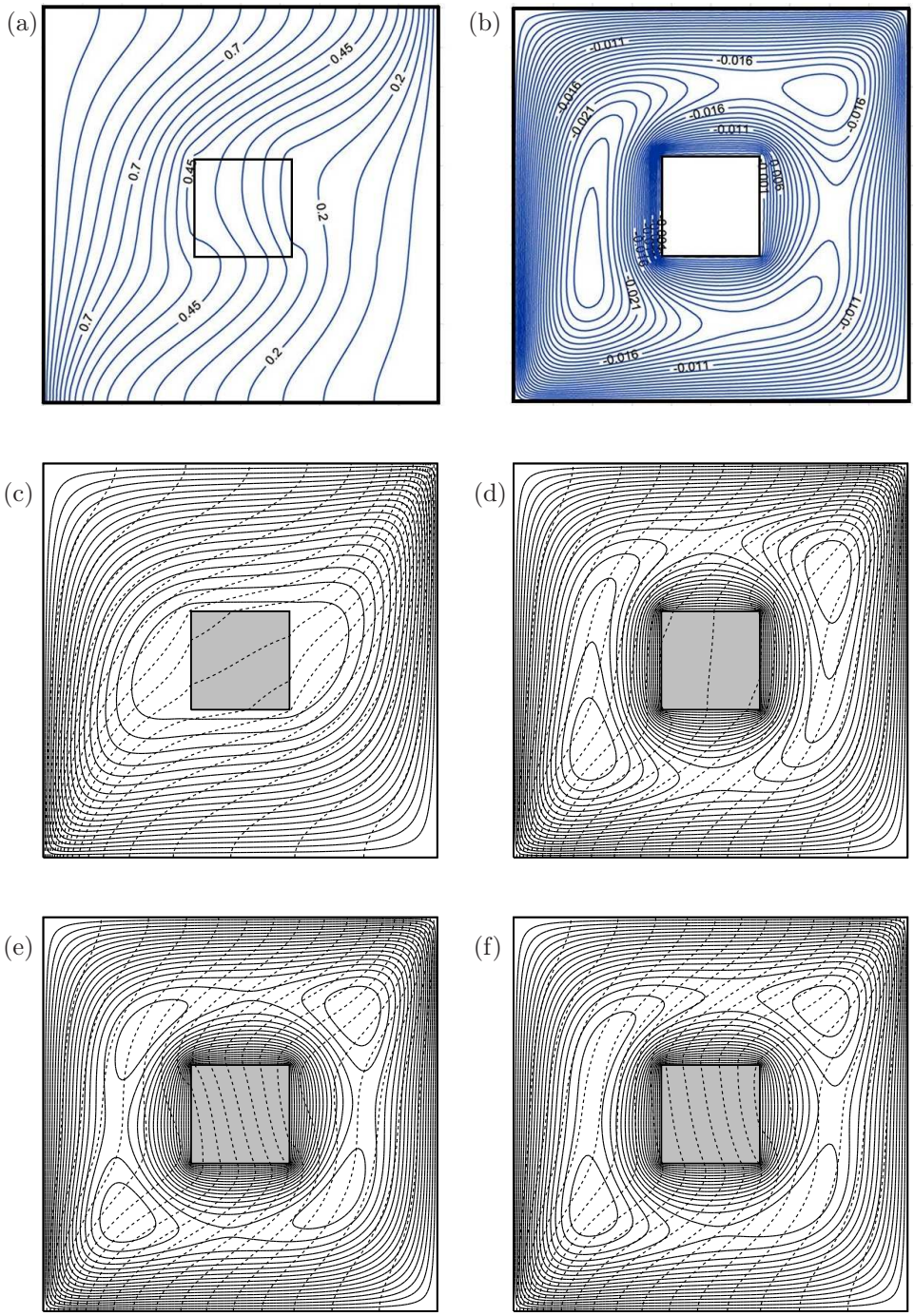

Figure 2. Showing the computed streamlines and isotherms for Ra = 100, $\kappa = 5$ and $\epsilon = 0.25$. (a) Isotherms and (b) streamlines from Nandalur et al. (2019). (c) Streamlines (continuous) and isotherms (dashed) for the present computation using a 120×120 uniform grid. (d) As (c) but with $\psi = 0$ imposed incorrectly on the surface of the solid block. (e) As (d) but with incorrect interface conditions on the upper and lower interfaces. (f) As (e) but with an incorrect left hand interface condition.

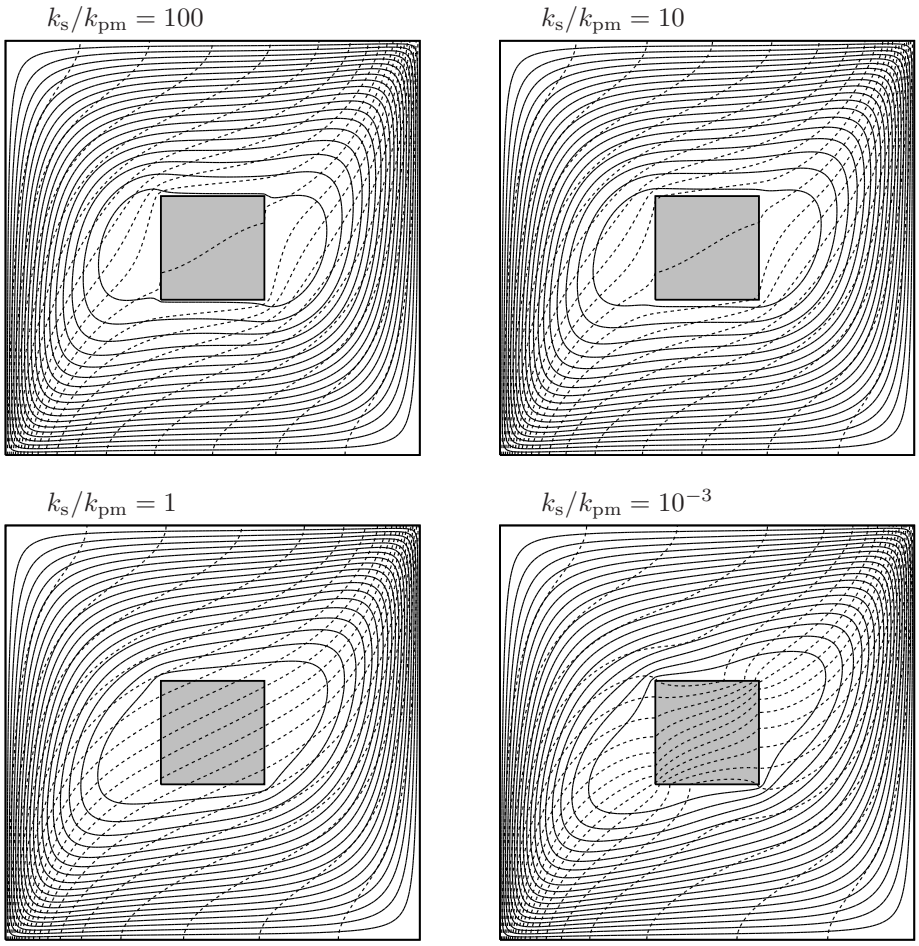

Figure 3. Showing the computed streamlines (continuous) and isotherms (dashed) for Ra = 100 and $\epsilon = 0.25$, and for the given selection of conductivity ratios. Here $N = 120$ with 20 equally-spaced streamlines and isotherms between their respective minima and maxima.

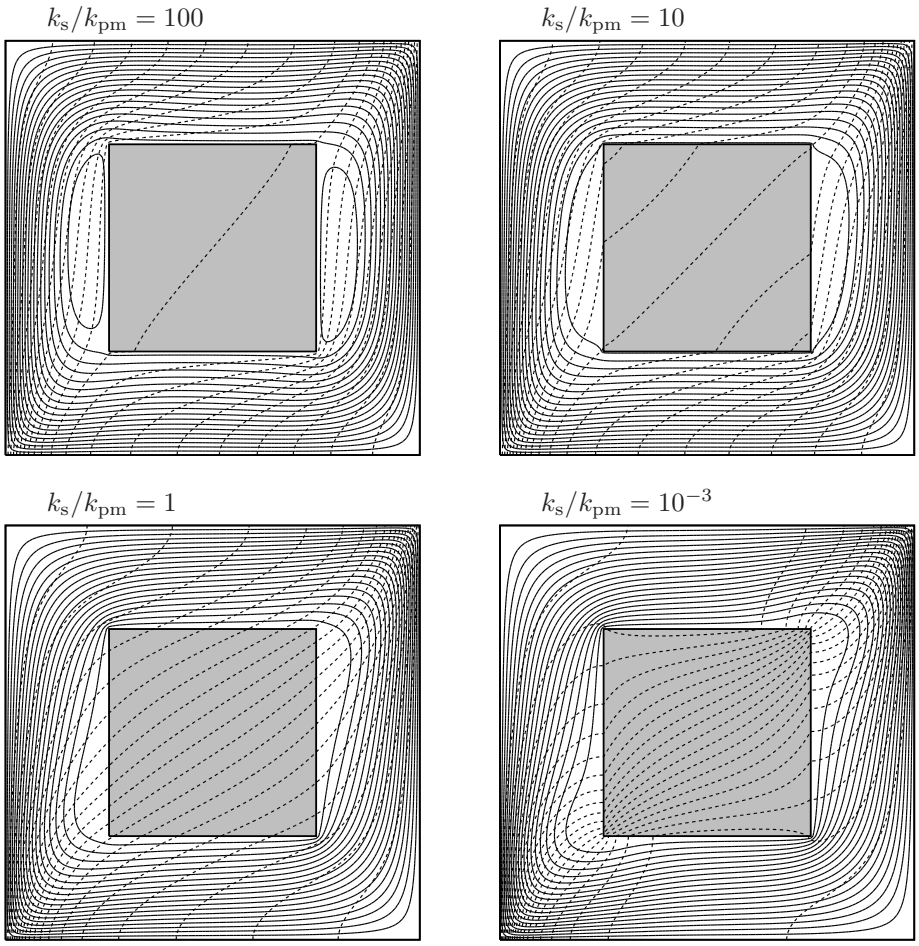

Figure 4. Showing the computed streamlines (continuous) and isotherms (dashed) for Ra = 100 and $\epsilon = 0.5$, and for the given selection of conductivity ratios. Here $N = 120$ with 20 equally-spaced streamlines and isotherms between their respective minima and maxima.

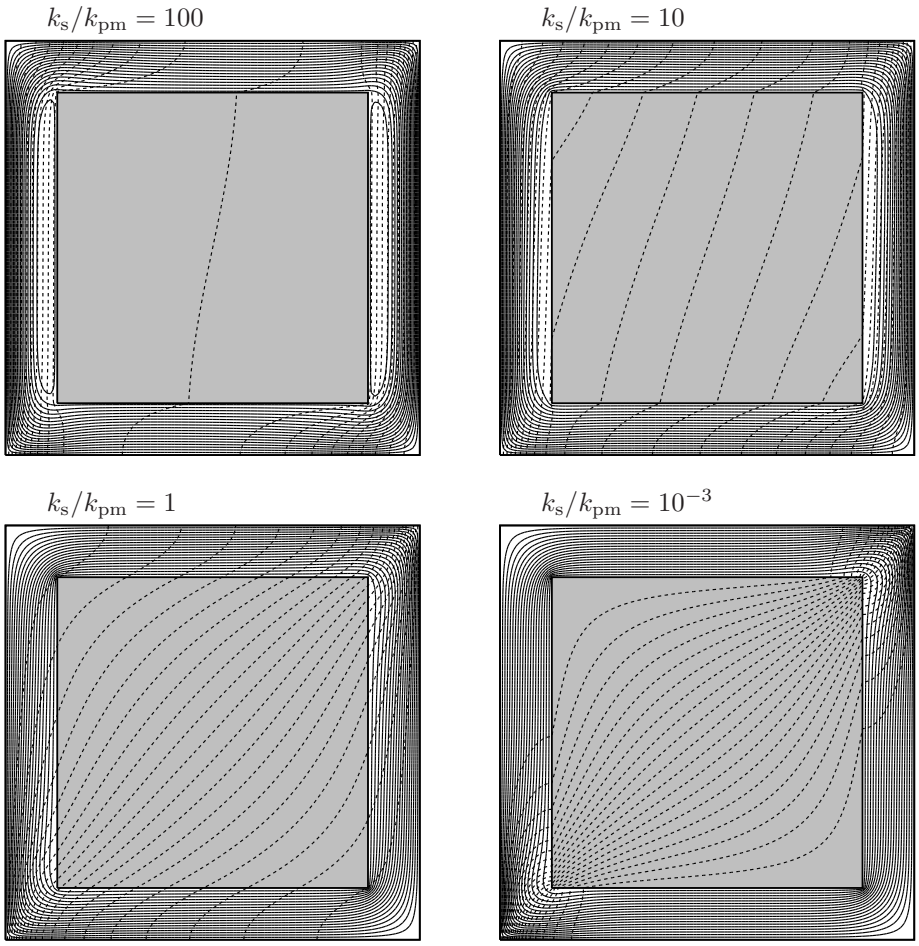

Figure 5. Showing the computed streamlines (continuous) and isotherms (dashed) for Ra = 100 and $\epsilon = 0.75$, and for the given selection of conductivity ratios. Here $N = 120$ with 20 equally-spaced streamlines and isotherms between their respective minima and maxima.

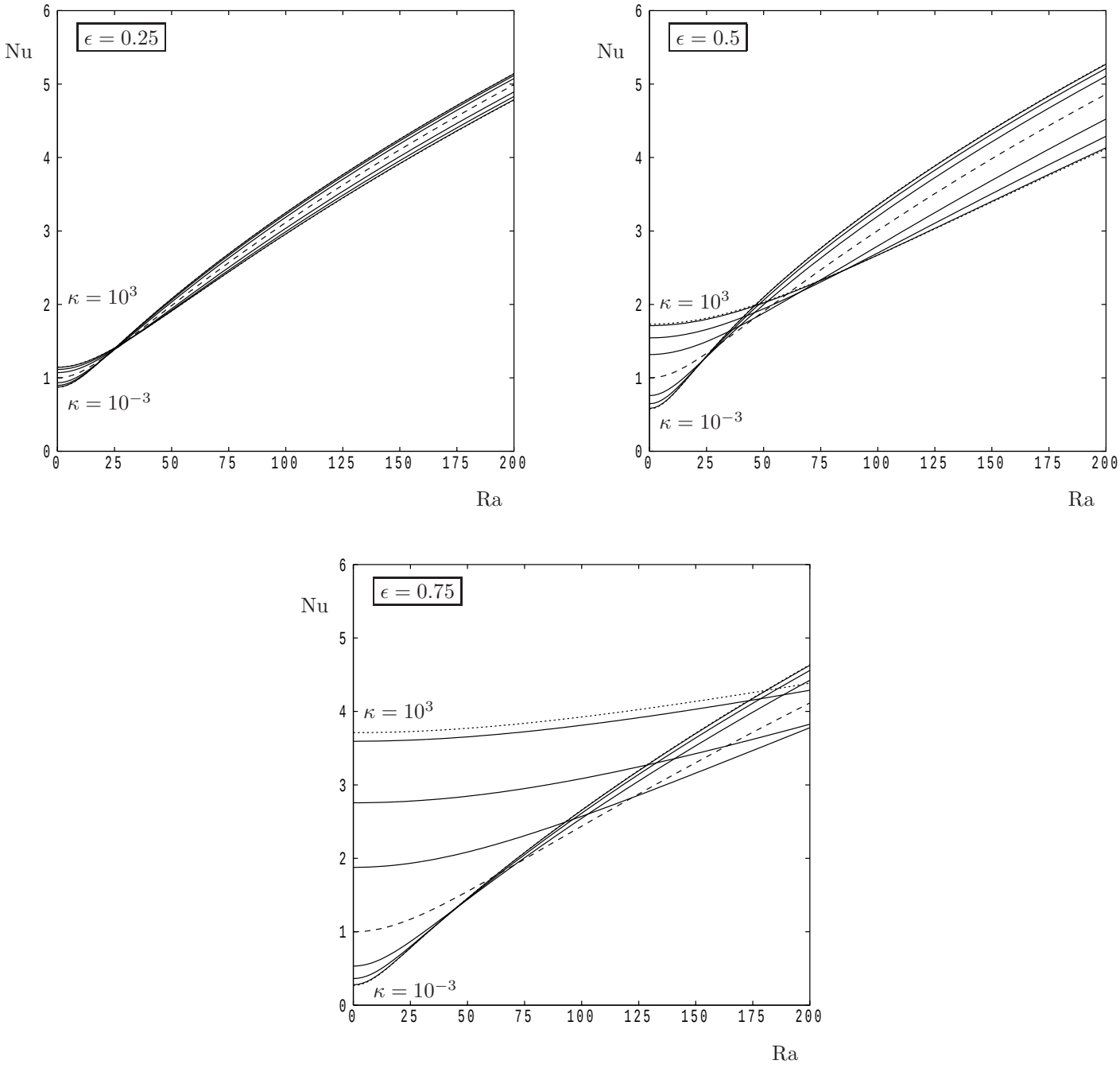

Figure 6. Showing the variation of Nu with the Darcy-Rayleigh number, Ra, for the given three values of ϵ and for the conductivity ratios, $\kappa = 10^{-3}$, 10^{-2}, 10^{-1}, $10^{-1/3}$, 10^{0}, $10^{1/3}$, 10^{1}, 10^{2} and 10^{3}. Dotted lines denote the two extreme cases while the dashed line denotes $\kappa = 1$. The solutions were obtained on a 120×120 grid.

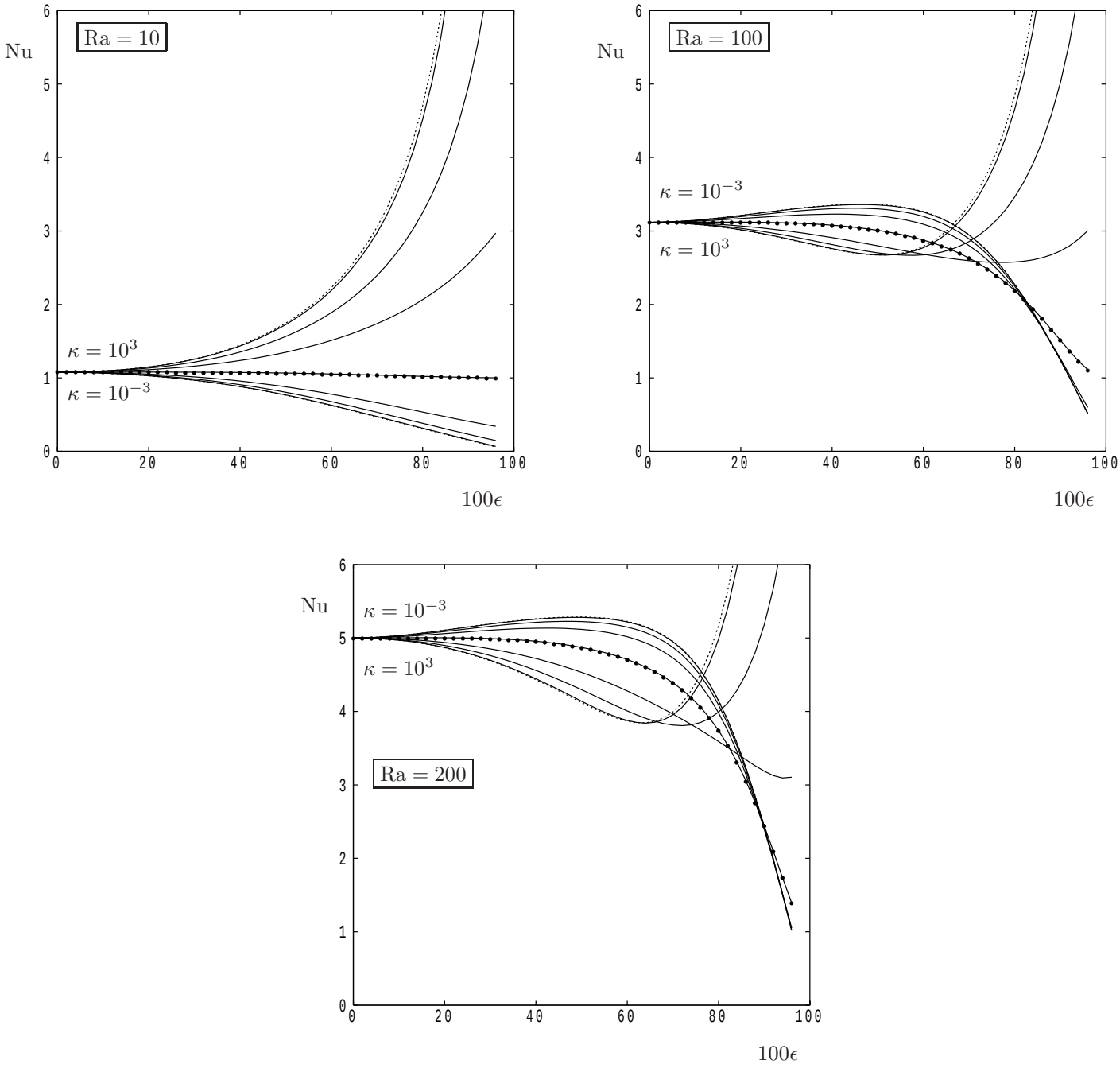

Figure 7. Showing the variation of Nu with the conductivity ratio, ϵ, for the three given values of Ra, and for the conductivity ratios, $\kappa = 10^{-3}$, 10^{-2}, 10^{-1}, $10^{-1/3}$, 10^{0}, $10^{1/3}$, 10^{1}, 10^{2} and 10^{3}. Dotted lines denote the two extreme cases while the line with the black discs denotes $\kappa = 1$. The solutions were obtained on a 100×100 grid; the horizontal axis gives ϵ as a percentage.